Supporting Information

Macroporous microspheres consisting of thickness-controlled bamboo-like CNTs and flower-like Co_3O_4 nanoparticles as highly efficient bifunctional oxygen electrocatalysts for Zn-air batteries

Sun Jun Kim,[†a] Jeong Hoo Hong,[†a] Jung-Kul Lee,[*b] and Yun Chan Kang[*a]

[a]Department of Materials Science and Engineering, Korea University, Anam-Dong, Seongbuk-Gu, Seoul 136-713, Republic of Korea.

[b]Department of Chemical Engineering, Konkuk University, Hwayang-dong, Gwangjin-gu, Seoul 143-701, Republic of Korea.

[†] These two authors contributed equally to this work.

[*]Corresponding author. E-mail: yckang@korea.ac.kr (Yun Chan Kang), jkrhee@konkuk.ac.kr (Jung-Kul Lee)

Experimental Section (Continued)

Characterization Techniques

The morphological characteristics of the samples were investigated by SEM (TESCAN, VEGA3) and HR-TEM (JEM-2100F) at a working voltage of 200 kV. The phase and crystal structures were analyzed using an X-ray diffractometer (X'Pert PRO) with Cu-Kα radiation (λ = 1.5418 Å) at the Korea Basic Science Institute (Daegu). The surface area and pore size distribution of the samples were analyzed using the BET (TriStar 3000) method. XPS (ESCALAB210) with Al Kα radiation was performed to investigate the molecular and chemical states of the microspheres. The structural characteristics of carbon in the samples were investigated via Raman spectroscopy (Jobin Yvon LabRam HR800, excited by a 515 nm diode laser). Thermogravimetric analysis (TGA, Pyris 1 Thermogravimetric Analyzer, Perkin Elmer) was conducted in the range of 0–800 °C at 5 °C min^{-1} under air.

ORR and OER measurements

The electrochemical activities of the ORR and OER were evaluated using an RDE (AFMSPCE, Pine Research Instrumentation) connected to a potentiostat (ZIVE SP1, WonATech Co., Ltd.) with a three-electrode electrochemical cell. The cell consisted of an electrocatalyst-coated glassy carbon electrode as the working electrode (GCE; 5 mm diameter), a graphite rod as the counter electrode, and a saturated calomel electrode (SCE) as the reference electrode. To prepare the working electrode, a homogeneous ink was prepared by dispersing the powders (10 mg) in 1 mL of a binary mixture of dimethylformamide and Nafion® (50 μL, 5 wt. %) via 30 min sonication. Subsequently, 10 μL of the fabricated ink was dropped onto the GCE and dried under an infrared lamp for 10 min, which had a mass loading of ~0.5 mg cm^{-2}. The mass loading of the benchmark electrocatalyst comprising Pt/C (20 %) and RuO_2 was ~0.5 mg cm^{-2}. For evaluating the ORR performance, LSV was performed at a rotation speed of 1600 rpm in O_2-saturated 0.1 M KOH with a scan rate of 10 mV s^{-1} in a potential window of 1.0 to 0.3 V vs RHE. The electrode potentials applied in these measurements were converted with reference to the reversible hydrogen electrode (RHE); these values were $E_{vs.}RHE = E_{vs.}RHE + 0.059\ pH + 0.097\ V$ and $E_{vs.}RHE = E_{vs.(Hg2/Cl2/Hg2,Cl-)} + 0.991\ V$ in 0.1 M KOH. The ECSA was estimated by measuring the capacitive current related to double-layer charging from the scan rate dependence of CV, which was performed on the same working

electrode in a certain non-Faraday region at scan rates ranging from 20 to 100 mV s^{-1}. C_{dl} was calculated by plotting Δj ($j_a - j_c$) at the middle point of the potential range against the scan rate. The ORR durability of the samples was investigated by their chronoamperometric responses at 0.80 V (vs. RHE) at a rotation speed of 1600 rpm in 0.1 M KOH for 20000 s, and the accelerated degradation test (ADT) was conducted at a scan rate of 10 mV s^{-1} in potential range of 0.65-1 V vs. RHE for 5,000 cycles. The OER performance was evaluated at a rotation rate of 1600 rpm in N_2-saturated 0.1 M KOH, with a scan rate of 10 mV s^{-1} in a potential window of 1.0 to 2.0 V vs RHE. LSV curves were recorded twice after the CV scan. The electrochemical impedance of the prepared samples was evaluated using electrochemical impedance spectroscopy over a frequency range of 100 kHz to 0.1 Hz, with a scan rate of 5 mV s^{-1}. The OER durability of the samples was investigated by the ADT at a scan rate of 10 mV s-1 in a potential window of 1.23 to 1.67 V vs. RHE for 1,000 cycles.

Manufacture and measurement of the ZABs

The electrocatalytic performance of Co/CNT_10Mg/Ni for the ZAB test was evaluated using a homemade cell. The electrocatalyst ink was prepared by dispersing 8.3 mg of powder in 825 μL of a binary mixed solution of ethanol (750 μL) and Nafion® (75 μL, 5 wt. %) via 30 min sonication. This solution was then released on carbon fiber paper and dried under an IR lamp for 1 h to prepare the air positive electrode with a loading of 1.0 mg cm-2. The mass loading of the benchmark consisting of Pt/C (20%) and RuO2 with a 1:1 ratio was 1.0 mg cm-2. The zinc plate was used as the negative electrode, and 6.0 M KOH with 0.2 M zinc acetate was used as the electrolyte. Polarization curves were recorded on an electrochemical analysis station (ZIVE SP1, WonATech Co., Ltd.), and the galvanostatic discharge and charge performance were tested on a WBCS3000s cycler (WonATech, Korea).

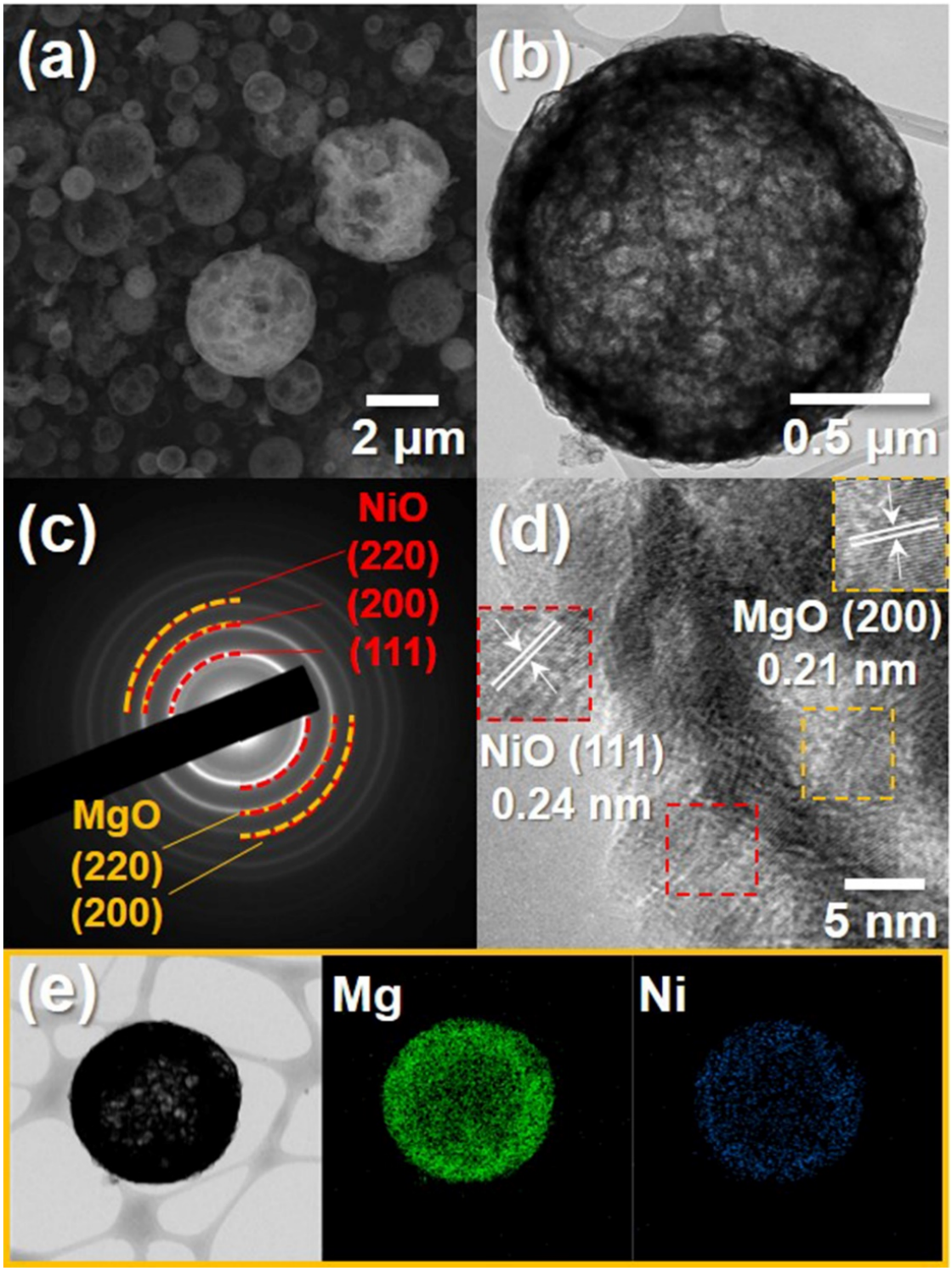

Fig. S1 Morphologies, SAED pattern, and elemental mapping images of MgO-NiO microspheres: (a) SEM image, (b) TEM image, (c) HR-TEM image, (d) SAED pattern, and (e) elemental mapping images.

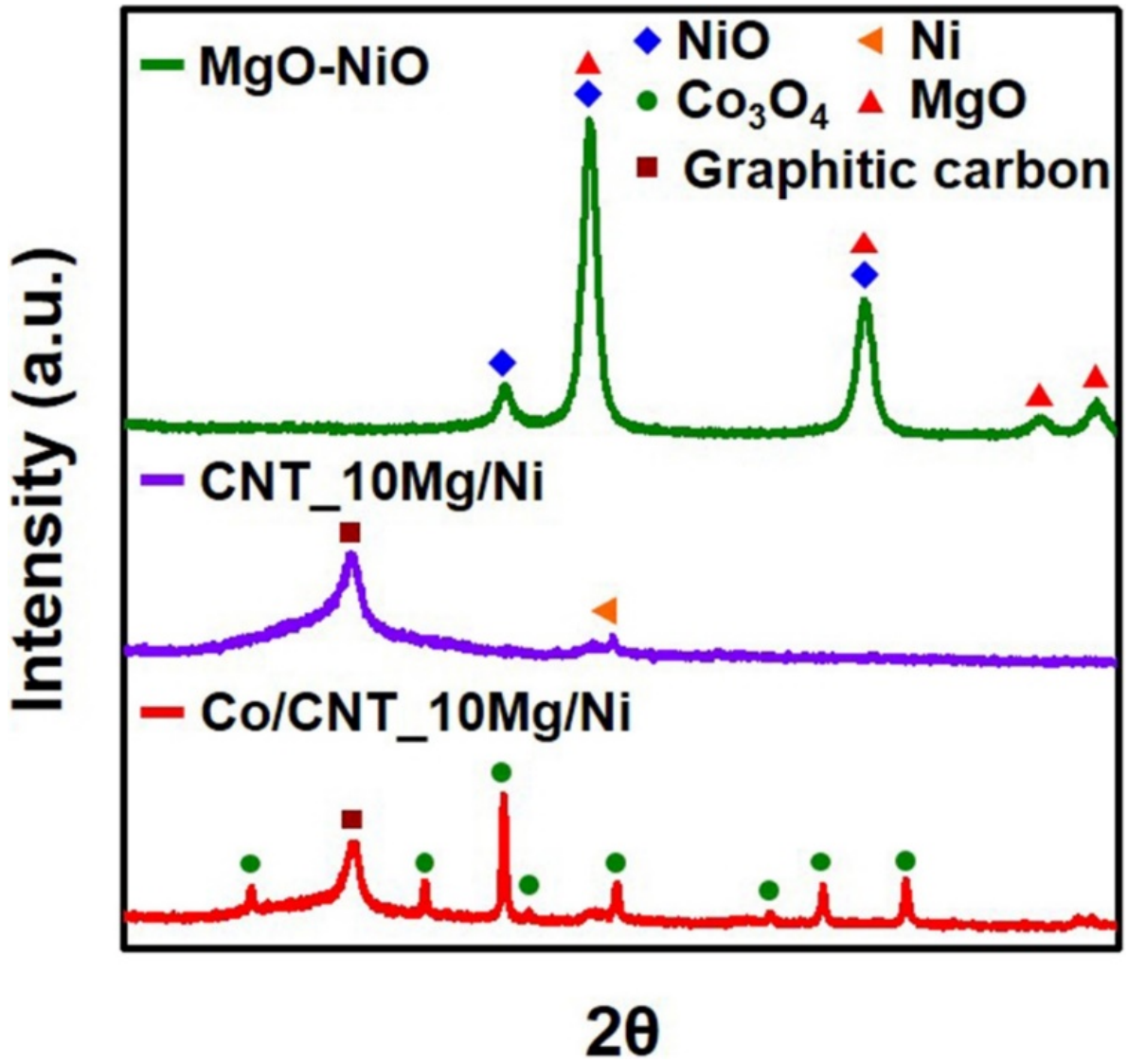

Fig. S2 XRD patterns of MgO-NiO, CNT_10Mg/Ni, and Co/CNT_10Mg/Ni.

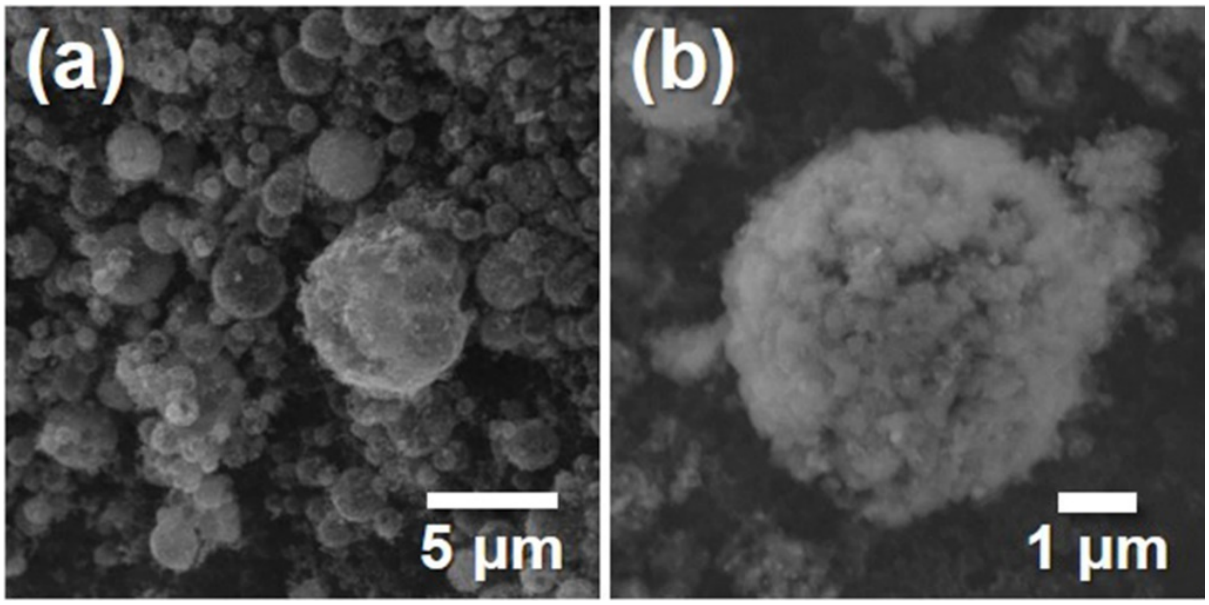

Fig. S3 SEM images of CNT_10Mg/Ni before MgO etching.

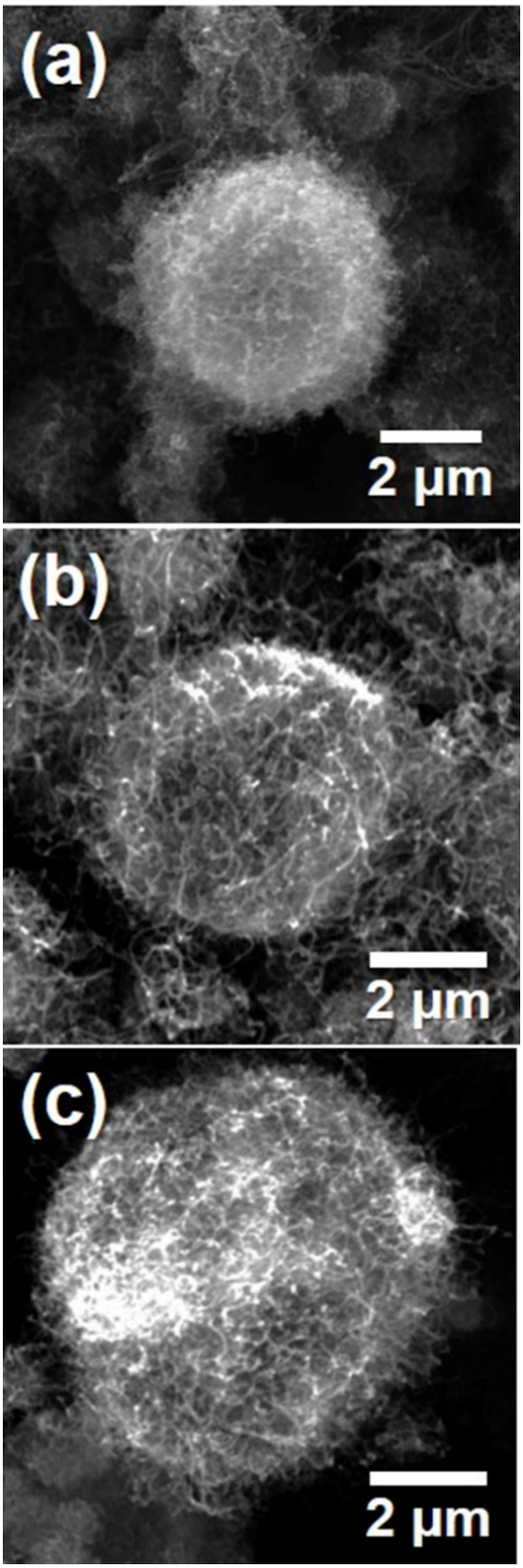

Fig. S4 SEM images of (a) CNT_1Mg/Ni, (b) CNT_3Mg/Ni, and (c) CNT_5Mg/Ni.

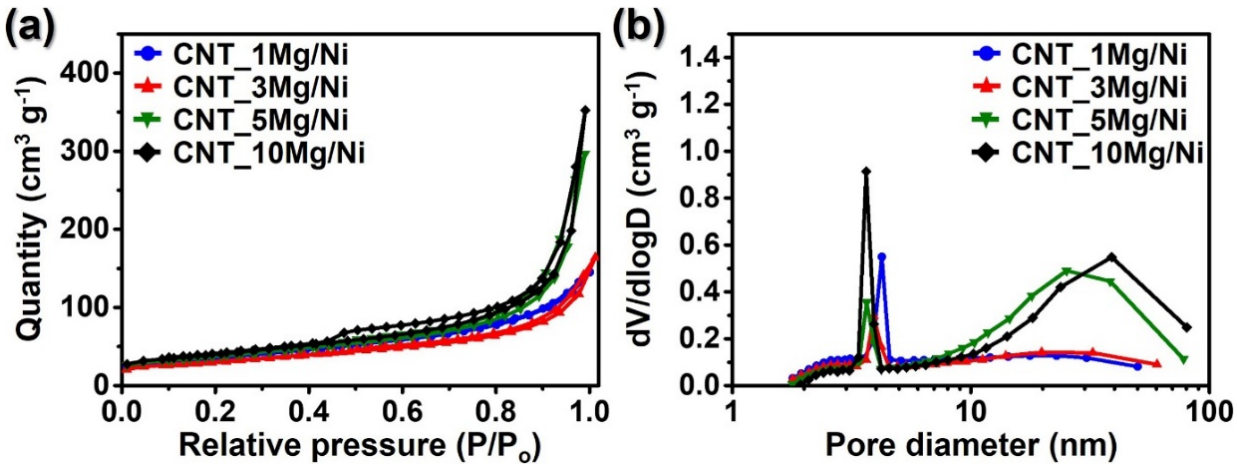

Fig. S5 (a) N_2 gas adsorption and desorption isotherms and (b) pore-size distributions of CNT_xMg/Ni.

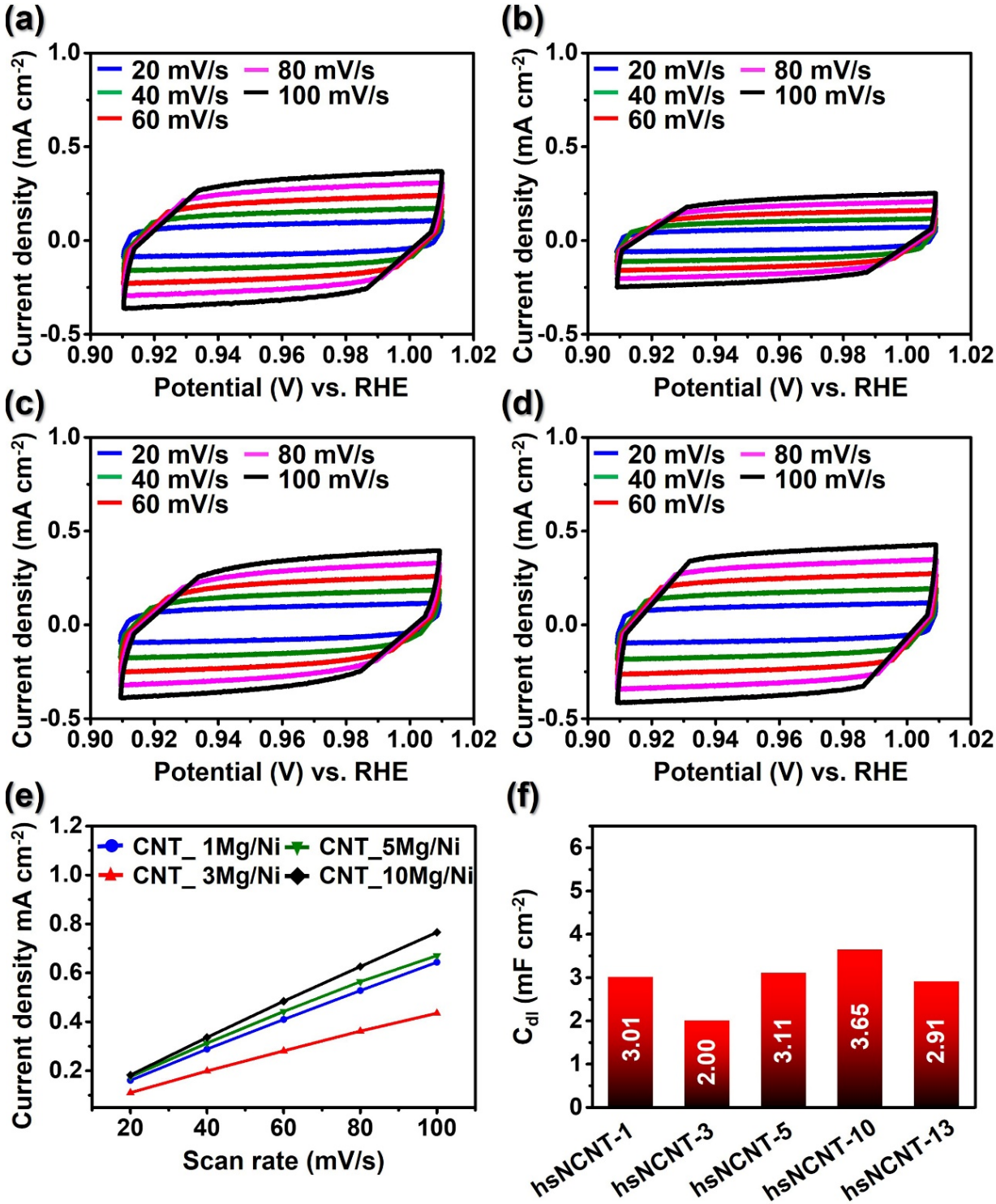

Fig. S6 Cyclic voltammetry curves of (a) CNT_1Mg/Ni, (b) CNT_3Mg/Ni, (c) CNT_5Mg/Ni, and (d) CNT_10Mg/Ni in the range between 0.92-1.01 V vs RHE with range from 20 to 100 mV s^{-1}, (e) corresponding linear fitting of the capacitive current densities, and (f) bar chart summarizing the C_{dl} values.

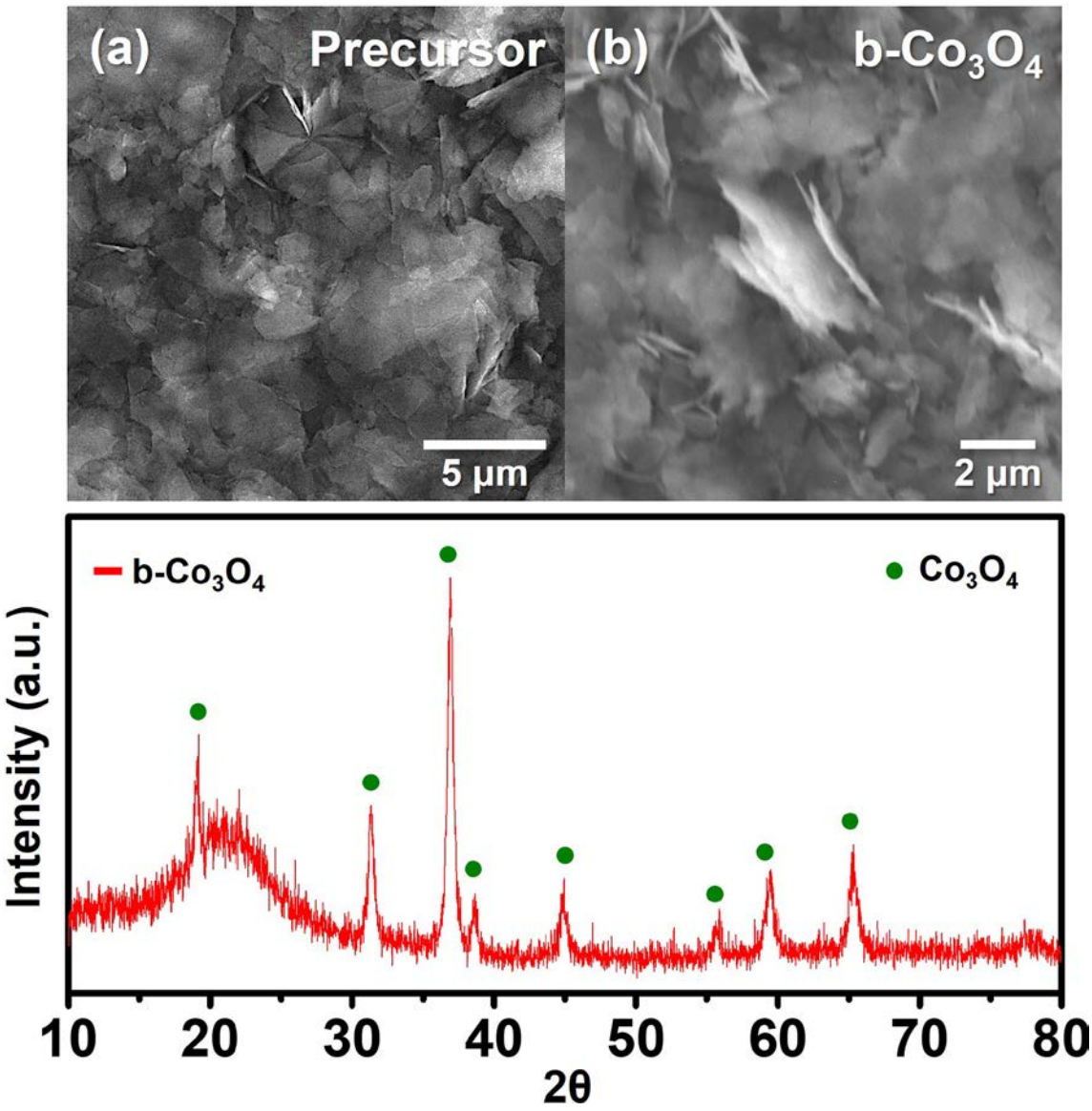

Fig. S7 SEM images of (a) the precursor and (b) b-Co_3O_4 and (c) XRD pattern of b-Co_3O_4.

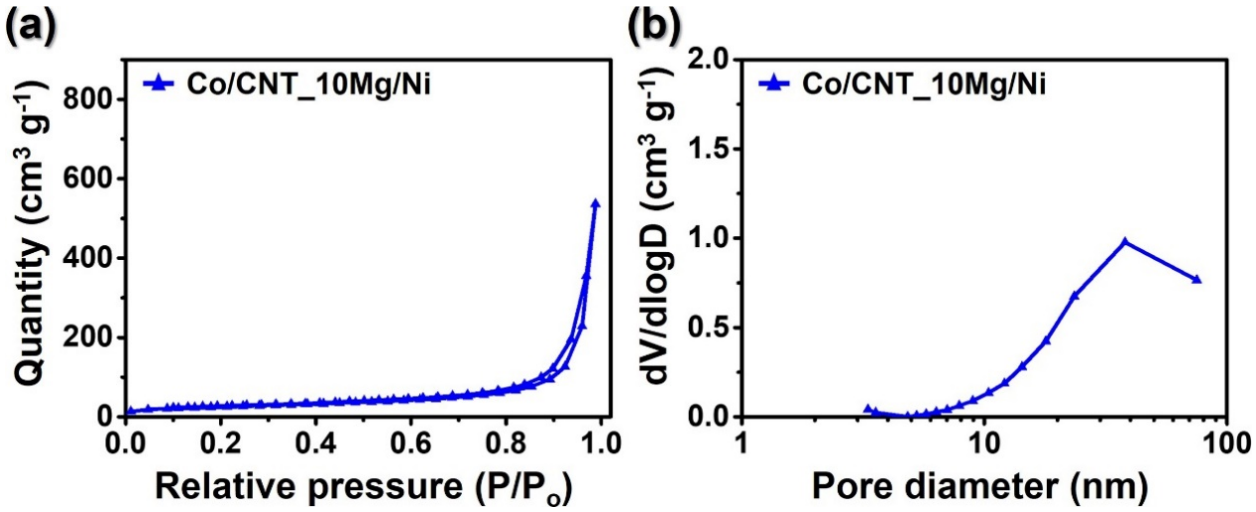

Fig. S8 (a) N_2 gas adsorption and desorption isotherm and (b) pore-size distribution of Co/CNT_10Mg/Ni.

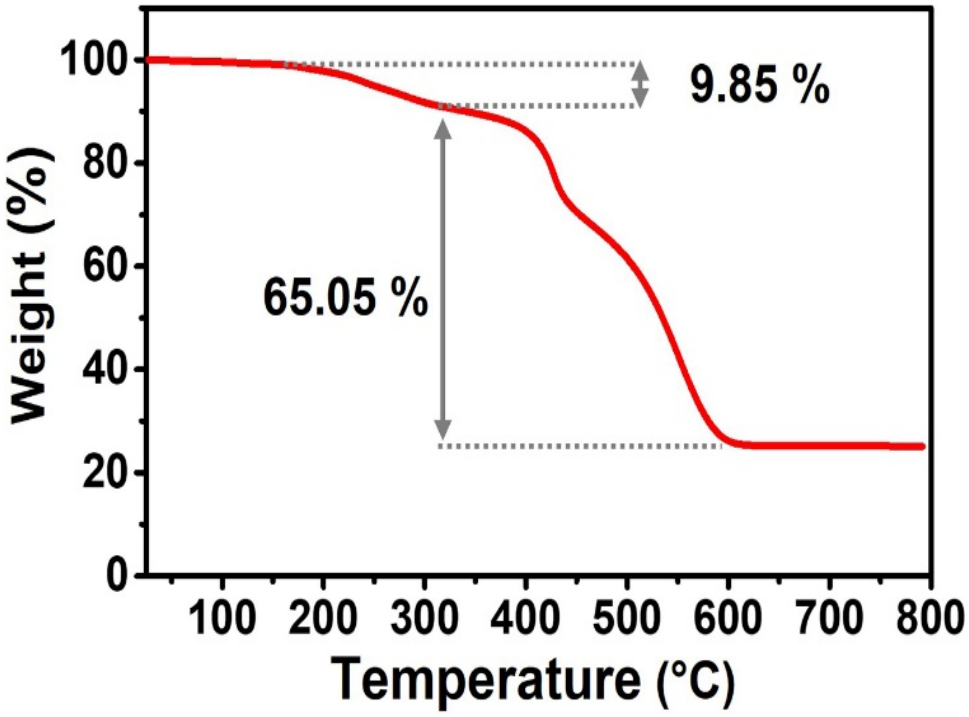

Fig. S9 TGA curve of Co/CNT_10Mg/Ni.

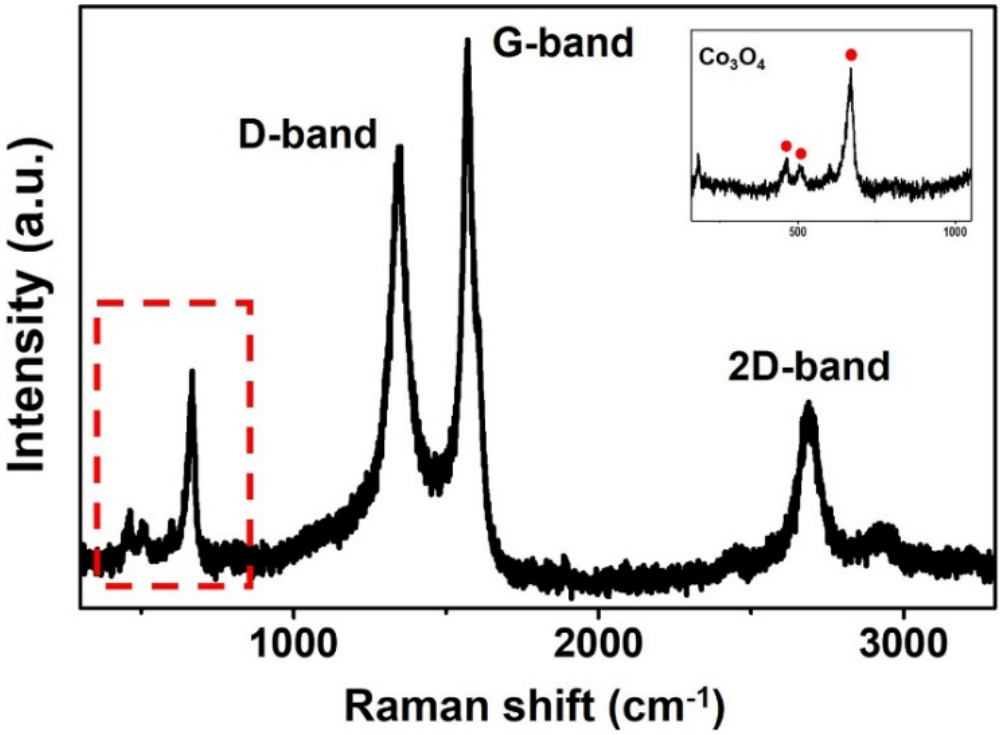

Fig. S10 Raman spectrum of Co/CNT_10Mg/Ni.

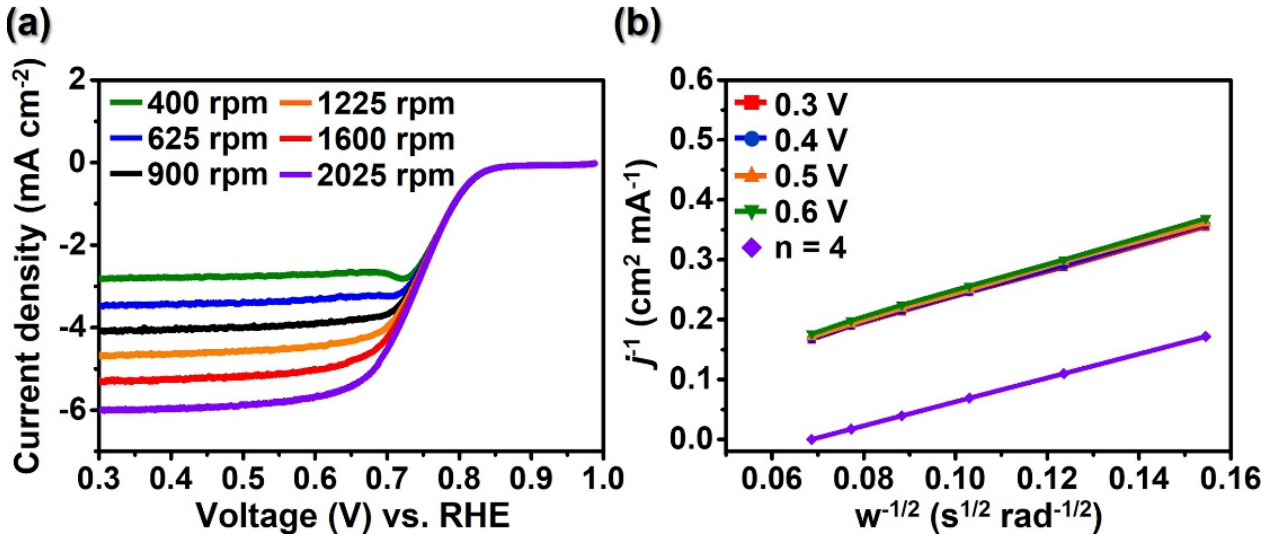

Fig. S11 (a) LSV curves for various rotating speeds and (b) the corresponding K-L plots for Co/CNT_10MgNi electrodes.

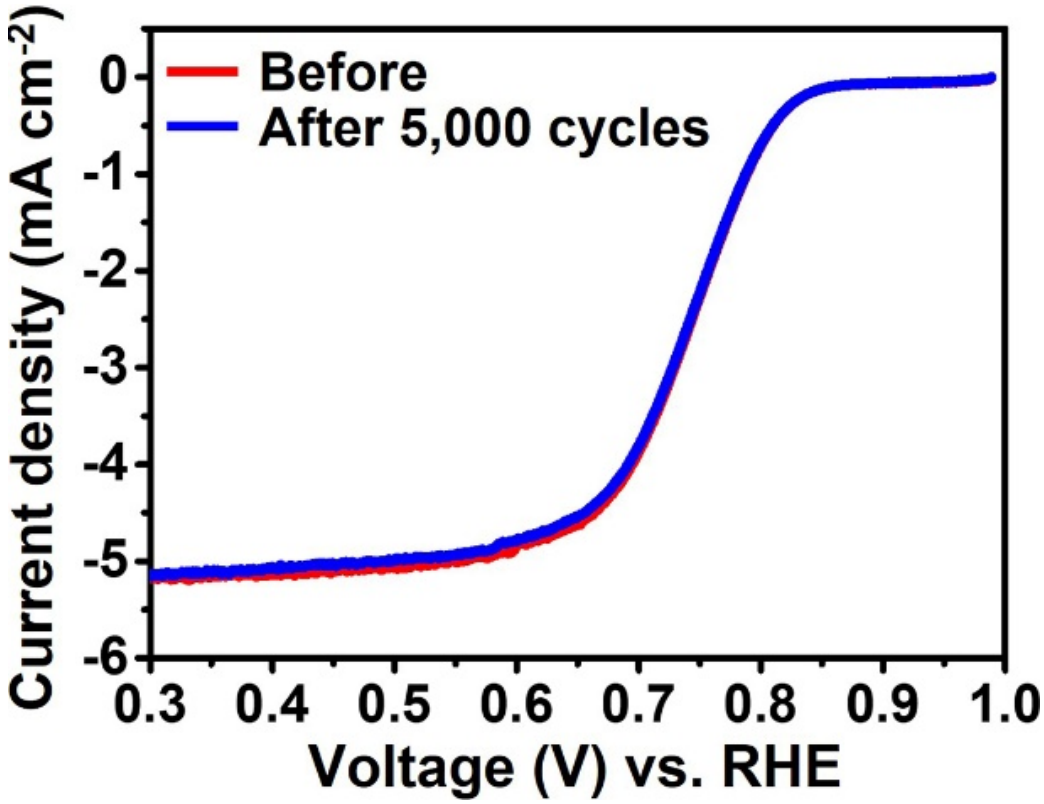

Fig. S12 LSV curves of Co/CNT_10Mg/Ni before and after 5,000 cycles for ORR.

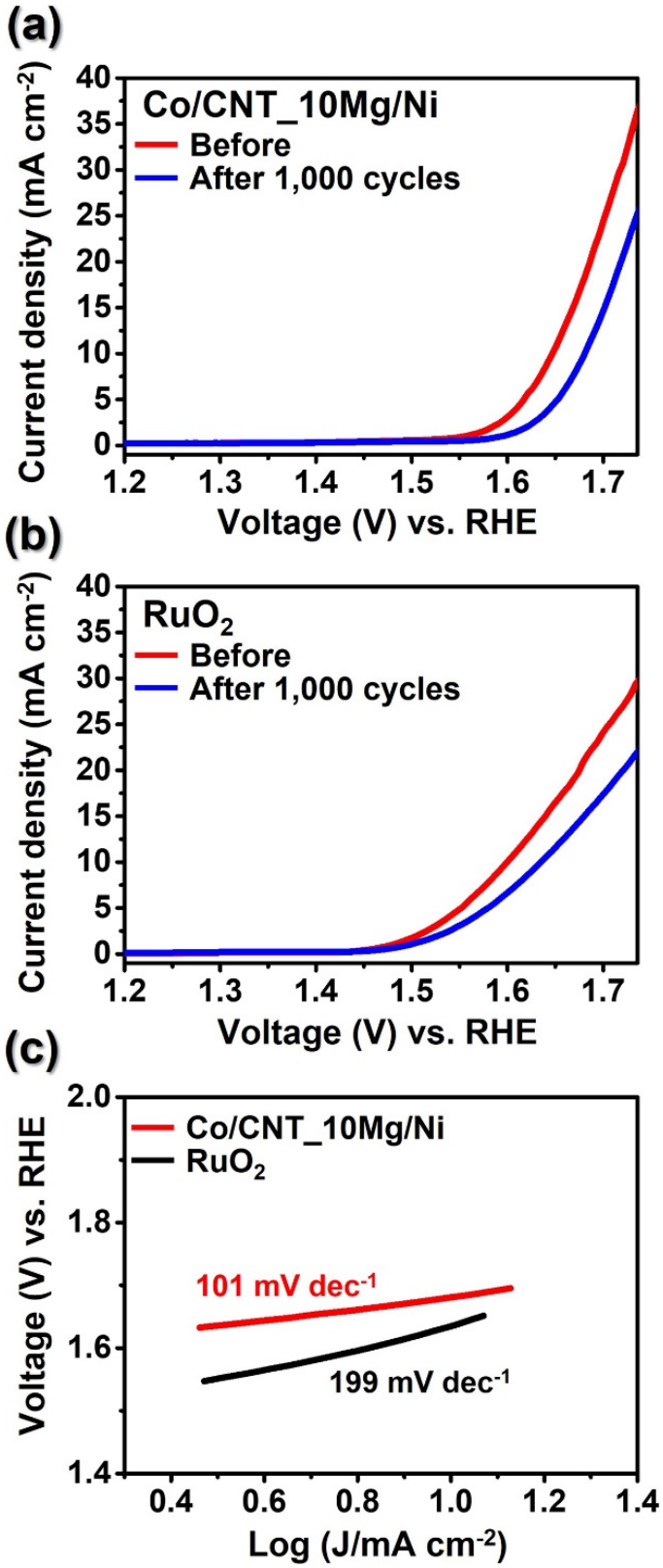

Fig. S13 LSV curves of (a) Co/CNT_10Mg/Ni and (b) RuO_2 before and after 1,000 cycles and (c) Tafel plots of Co/CNT_10Mg/Ni and RuO_2 after 1,000 cycle

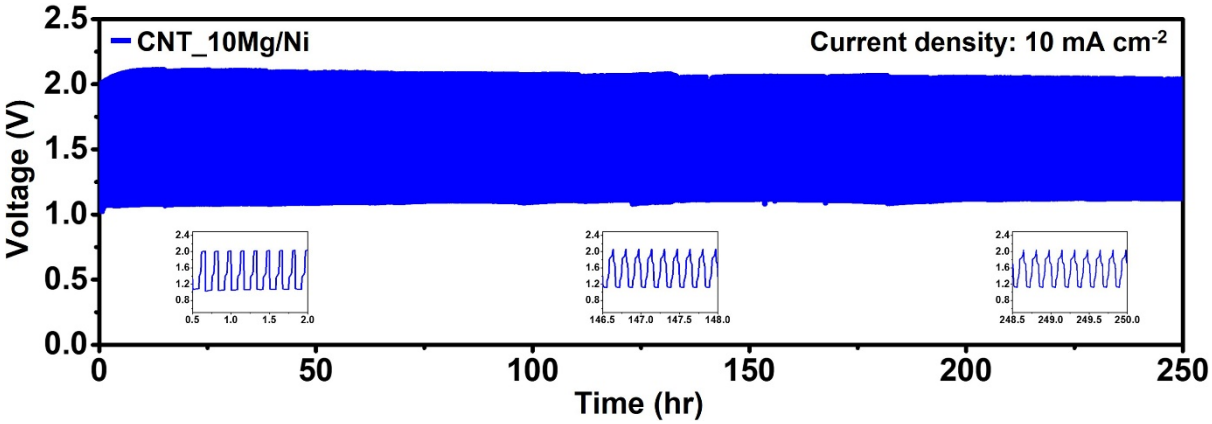

Fig. S14 Galvanostatic discharge and charge tests of CNT_10Mg/Ni.

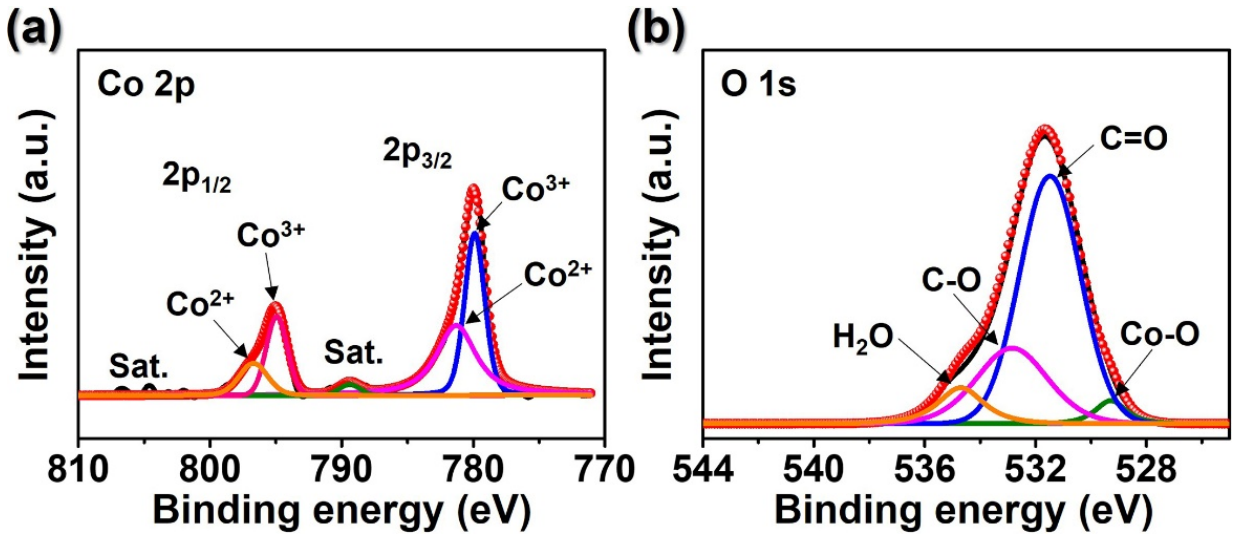

Fig. S15 XPS spectra of Co/CNT_10Mg/Ni obtained after Zn-air battery testing: (a) Co 2p and (b) O 1s.

Table S1 Zn-air battery performances of various transition metal oxide/N-doped carbon hybrid catalysts for air cathode reported in the previous studies.

Electrocatalysts	Loading ($mg\ cm^{-2}$)	Maximum power density ($mW\ cm^{-2}$)	Voltage gap	Electrolyte	Ref
Co_3O_4-Co heterostructure embedded in Co, N co-doped carbon polyhedra	0.2	158	1.2 (10 mA cm^{-2})	6 M KOH + 0.2 M Zn acetate	[1]
Two trifunctional electrocatalysts composed of Ni–NiM_2O_4 (M = Mn or Fe) supported on N-doped carbon	1.0	105	N/A	6 M KOH	[2]
Fe^{3+} doping in Co_3O_4 spinel nanoparticles grown on N-doped carbon nanotubes.	0.90	90.68	1.23 V (50 mA cm^{-2})	6 M KOH + 0.2 M Zn acetate	[3]
Nitrogen-doped graphitic carbon-encapsulated MnO-Co heterostructure supported on onion-like carbon	1.13	86	0.98 V (5 mA cm^{-2})	6 M KOH + 0.2 M Zn acetate	[4]
Co^{2+}-activated spinel $CoMn_2O_4$ supported self-catalysis derived nitrogen-doped carbon nanotubes	9.0	79.86	N/A	6 M KOH + 0.2 M Zn acetate	[5]
Combination of the MnO and metallic Ni with N- doped carbon (N–C) materials	1.0	179	N/A	6.0 M KOH	[6]
Co_3O_4–$NiCo_2O_4$ anchored on N-doped reduced graphene oxide nanosheets	1.0	97	0.79 (10 mA cm^{-2})	6 M KOH + 0.2 M Zn acetate	[7]
1D/2D hierarchical $Co_{1-x}Fe_xO$@NC nanostructures directly grown on the carbon cloth	0.1	52	0.97 (5 mA cm^{-2})	6 M KOH + 0.2 M Zn acetate	[8]
Metallic Co cores decorated with Co_3O_4 semiconductive shells are embedded in N-doped carbon	1.0	135	1.98 (5 mA cm^{-2})	6 M KOH + 0.2 M Zn acetate	[9]
Ingenious Co single atom anchored on $Co_3O_4$and nitrogen-doped active carbon	1.3	164	0.791 (10 mA cm^{-2})	6 M KOH + 0.2 M Zn acetate	[10]
Co/CNT_10Mg/Ni	**1.0**	**181**	**0.85 V (10 mA cm^{-2})**	**6 M KOH + 0.2 M Zn acetate**	**This work**

References

[1] Z. Zhang, Y. Tan, T. Zeng, L. Yu, R. Chen, N. Cheng, S. Mu and X. Sun, *Nano Res.*, 2020, 1-10.

[2] Q. Qin, L. Chen, T. Wei, Y. Wang and X. Liu, *Catal. Sci. Technol.*, 2019, **9**, 1595-1601.

[3] X. T. Wang, T. Ouyang, L. Wang, J. H. Zhong, T. Ma and Z. Q. Liu, *Angew. Chem.*, 2019, **131**, 13425-13430.

[4] A. Samanta, B. K. Barman, S. Mallick and C. R. Raj, *ACS Appl. Energy Mater.*, 2020, **3**, 10108-10118.

[5] H. Su, X.-T. Wang, J.-X. Hu, T. Ouyang, K. Xiao and Z.-Q. Liu, *J. Mater. Chem. A*, 2019, **7**, 22307-22313.

[6] H. Zhang, Z. Lu, B. Liu, S. Wang and Y. Cao, *J. Power Sources*, 2021, **485**, 229330.

[7] Z. Zhu, J. Zhang, X. Peng, Y. Liu, T. Cen, Z. Ye and D. Yuan, *Energy Fuels*, 2021, **35**, 4550-4558.

[8] Y. Chong, Z. Pan, M. Su, X. Yang, D. Ye and Y. Qiu, *Electrochim. Acta*, 2020, **363**, 137264.

[9] T. Singh, C. Das, N. Bothra, N. Sikdar, S. Das, S. K. Pati and T. K. Maji, *Inorg. Chem.*, 2020, **59**, 3160-3170.

[10] X. Zhong, W. Yi, Y. Qu, L. Zhang, H. Bai, Y. Zhu, J. Wan, S. Chen, M. Yang and L. Huang, *Appl. Catal., B*, 2020, **260**, 118188.